Tool Wear Monitoring of Wiper Inserts in Multi-Insert Face Milling Using Three-Dimensional Surface Form Indicators

Data · August 2015

CITATIONS
4

READS
55

4 authors, including:

Meng Wang
Shanghai Jiao Tong University
7 PUBLICATIONS **25** CITATIONS
SEE PROFILE

Shichang Du
Shanghai Jiao Tong University
49 PUBLICATIONS **297** CITATIONS
SEE PROFILE

Lifeng Xi
Shanghai Jiao Tong University
180 PUBLICATIONS **1,687** CITATIONS
SEE PROFILE

Meng Wang[1]
State Key Laboratory of Mechanical System and Vibration,
Department of Industrial Engineering and Logistics Management,
School of Mechanical Engineering,
Shanghai Jiao Tong University,
800 Dongchuan Road,
Shanghai 200240, China
e-mail: mwang@sjtu.edu.cn

Te Ken
State Key Laboratory of Mechanical System and Vibration,
Department of Industrial Engineering and Logistics Management,
School of Mechanical Engineering,
Shanghai Jiao Tong University,
800 Dongchuan Road,
Shanghai 200240, China
e-mail: kente@sjtu.edu.cn

Shichang Du
State Key Laboratory of Mechanical System and Vibration,
Department of Industrial Engineering and Logistics Management,
School of Mechanical Engineering,
Shanghai Jiao Tong University,
800 Dongchuan Road,
Shanghai 200240, China
e-mail: lovbin@sjtu.edu.cn

Lifeng Xi
State Key Laboratory of Mechanical System and Vibration,
Department of Industrial Engineering and Logistics Management,
School of Mechanical Engineering,
Shanghai Jiao Tong University,
800 Dongchuan Road,
Shanghai 200240, China
e-mail: lfxi@sjtu.edu.cn

Tool Wear Monitoring of Wiper Inserts in Multi-Insert Face Milling Using Three-Dimensional Surface Form Indicators

The wear of wiper inserts directly affects the finishing surface quality in multi-insert face milling. This research aims at monitoring the wear of wiper inserts, using 3D surface form as tool wear indicators. 3D surface height map of the face-milled surface is measured by a high definition metrology (HDM) instrument and converted into height-encoded and toolmark-straightened gray images. 3D surface form indicators, including entropy and contrast, are extracted from the converted images with a modified gray level co-occurrence matrix (GLCM) method. Meanwhile, the wear of wiper inserts is measured using a tool presetter and measuring machine without dismounting wiper inserts from the cutter. Experimental results indicate that entropy shows a strong correlation with average axial wear of the wiper edges and contrast reflects the evolution of axial offset between wiper inserts. [DOI: 10.1115/1.4028924]

Keywords: tool wear, wiper insert, high definition metrology, gray level co-occurrence matrix

1 Introduction

Cutting tool wear has a direct impact on product quality, production efficiency, and tool change cost. Therefore, monitoring tool wear is essential to ensure cutting tools in satisfactory condition and reduce downtime and tool costs [1].

Methods for tool wear monitoring have been extensively studied. These methods consist of two categories: direct methods and indirect methods. Direct methods measure actual geometric changes of cutting edge using machine vision [2–6] or scanning electron microscope (SEM) [7] directly. However, direct methods are influenced by illumination condition, reflectance of tool edge, coolant mist, and efficiency. Indirect methods take advantage of related signals as tool wear indicators, such as cutting force [8,9], torque [10], vibration [11,12], drive parameters [13,14], and acoustic emission [15,16]. Among indirect methods, using surface texture as tool wear indicators has long been a matter of interest. Because tool wear affects the surface texture of the final parts [17]. In other words, the texture of the machined surface is a replica of the changing of the cutting tool shape [18]. Furthermore, the primary factor that results in degradation of surface finish and form accuracy is the change of cutting tool shape under stable machining condition [19]. Therefore, surface texture can provide reliable and detectable information for tool wear monitoring.

Surface texture used for tool wear monitoring mainly comes from three kinds of measuring techniques: (a) contacting stylus techniques, (b) machine vision techniques, and (c) noncontacting optical techniques. Contacting stylus techniques can directly measure surface texture, such as roughness and waviness, for tool condition monitoring [20]. However, despite of the high measuring accuracy, contacting stylus techniques are highly localized and are difficult for online application. Machine vision techniques extract surface texture parameters from the obtained images. With rapid image capturing speed, machine vision systems are qualified for online tool wear monitoring. A thorough review of image texture analysis methods for tool condition monitoring can be found in Ref. [21]. However, extracting surface texture using machine

[1]Corresponding author.

Contributed by the Manufacturing Engineering Division of ASME for publication in the Journal of Manufacturing Science and Engineering. Manuscript received May 11, 2014; final manuscript received October 17, 2014; published online February 18, 2015. Assoc. Editor: Robert Gao.

version is not straightforward as surface texture is predicted by captured surface images indirectly. The image quality is influenced by nonuniform illumination, depth of focus, and noises (dirt, cut chips, etc.) in the industrial environment. Noncontacting optical techniques, such as phase-shifting interferometry, coherence scanning interferometry, and atomic force microscopy, can achieve accurate 3D surface measurement directly [22]. Some of these techniques have huge potentials for online tool condition monitoring due to fast measurement speed. However, these techniques usually have a small field of view so that they cannot reveal the subtle textural changes of the entire surface.

Due to a lack of metrology that is able to measure large surfaces with high resolution, tool wear monitoring using 3D surface information of the entire surface has seldom been studied. A recent advancement of noncontact optical technique, HDM, gains the ability to measure 3D surface height map of the entire surface at sub-μm level within 40 s [23]. For example, as shown in Fig. 1, the engine block surface measured by HDM including about 0.8×10^6 data points covers an area of 320 mm $\times$ 160 mm with 0.15 mm resolution in x–y direction and 1 μm accuracy in depth direction. Therefore, the 3D surface topography of the entire surface examined by HDM presents a novel platform for online tool condition monitoring. Liao et al. [24] used 2D Gaussian filter to extract 3D surface waviness of machined to access flank wear of a single cutting insert. In order to avoid boundary distortion, a minimum evaluation area is required when using 2D fillers. However, discontinuous surfaces like engine block surfaces with cylinder holes, bolt holes, and cooling holes, do not always have the continuous large enough area for 2D filtering operations. 3D surface form features introduced in Ref. [25] can describe the 3D height and spatial information of the entire discontinuous surface measured by HDM, which serve as a promising tool to monitor the wear of wiper inserts. Nevertheless, for multi-insert face milling with cutting inserts and wiper inserts in the same cutter, surface finish quality depends more on wiper inserts than cutting inserts. Therefore, this research aims to monitor the wear of wiper inserts in multi-insert face milling using 3D surface form indicators.

The remainder of this paper is organized as follows: Sec. 2 describes the experimental setup of multi-insert face milling and the wear measurement of wiper inserts. Section 3 presents a method on extraction of wear indicators from 3D surface height map measured by HDM. Experimental results and discussions are given in Sec. 4. Finally, Sec. 5 draws conclusions and discusses future research.

2 Measurement of Wiper-Insert Wear

An experiment on engine blocks was performed to study the wear of wiper inserts in a multi-insert face milling. Engine block surfaces were machined by a KNOLL KF400 machining center. The engine block material is FC250 cast iron with the following chemical composition: 3.0–3.4% C, 1.9–2.4% Si, 0.66–0.9% Mn, 0.2–0.5% Cr, 0.3–0.8% Cu, 0.15%S, 0.10%P. Quaker 370 KLG cutting fluid was used. Cutting parameters were set the same as those parameters for the production line: the depth of cut was 0.5 mm, the cutting speed was 1300 rpm, and feed rate was 3360 mm/min.

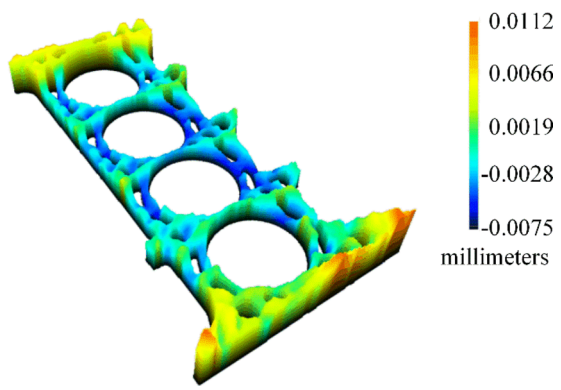

Fig. 1 3D surface height map measured by HDM

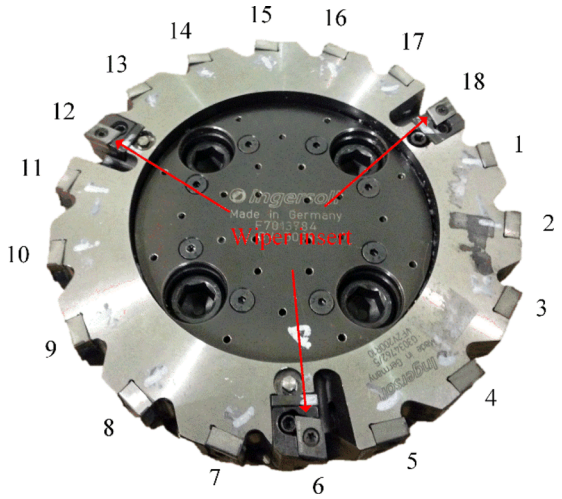

Fig. 2 The face milling cutter with 15 cutting inserts and 3 wiper inserts

The face milling cutter has a diameter of 200 mm with 15 cutting inserts intercalated by three wiper inserts. As shown in Fig. 2, inserts 1–5, 7–11, and 13–17 are the cutting inserts and inserts 6, 12, and 18 are the wiper inserts. The cutting tool material for the wiper insert is PCBN. The cutting inserts and wiper inserts were mounted based on the following criterion. The maximum admissible axial deviation between the three wiper inserts was 0.003 mm. The cutting inserts were installed between 0.02 mm to 0.06 mm below the lowest wiper insert. Table 1 shows the cutting angles of the cutting inserts and wiper inserts.

We measured worn wiper inserts using a Hitachi SEM S-3400 N to identify the predominant wear modes. Figure 3 shows the flank face and the rake face of the worn wiper insert. The dominant wear patterns within the normal life period were observed to be microcracks and axial lowering of the wiper edge. The microcracks, which combine the wear on the flank face and rake face, are adjacent to the wiper edge. This is because the cutting force is concentrated adjacent to the wiper edge as the insert-chip contact length for wiper inserts is short. Adhesion and abrasion are also considered to be the wear mechanism for PCBN wiper inserts [26]. The lowering of the wiper edge in the direction parallel to the axis of the cutter could be caused by plastic deformation or plastic lowering due to high temperature creep and could be the predominant cause of premature tool failure [27].

However, the inserts had to be dismounted from the cutter to measure the subtle wear of wiper inserts using SEM or tool maker's microscope. The disengagement and engagement of the inserts and the cuter will result in mounting error, which will alter the normal wear process of the wiper inserts in subsequent operations. To tackle this problem, we use ZOLLER Venturion 600, a

Table 1 Geometry of cutting inserts and wiper inserts

Tool geometry	Cutting inserts	Wiper inserts
Radial rake angle	0 deg	−16 deg
Axial rake angle	9 deg	0.2 deg
Cutting edge angle	90 deg	90 deg
Minor cutting edge angle	0 deg	4 deg
Inclination angle	9 deg	0.2 deg
Tip radius	0.8 mm	1 mm

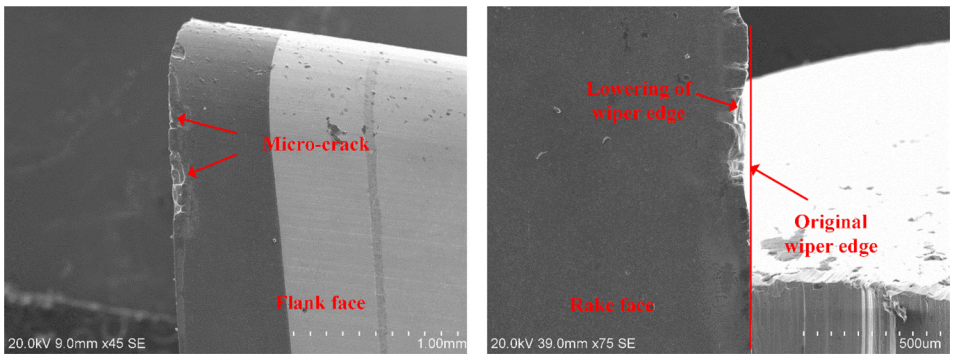

Fig. 3 Wear of wiper inserts

tool presetter and measuring machine, to measure the axial positions of all inserts without dismounting the inserts from the cutter. Then the lowering of the wiper edge is calculated as the changes of axial positions of wiper edges.

As we mainly focus on monitoring the tool wear in normal production, the number of machined engine blocks is set at 350, which is the preset tool life span. Axial positions of all inserts were measured every 50 engine blocks. Figure 4(*a*) shows the measured axial positions of the three wiper insert 6, 12, and 18. However, we found that the present axial positions could be higher than previously measured axial positions. For example, the axial positions of the wiper inserts after machining 50 engine blocks are higher than the initial axial positions. This phenomenon is not consistent with common scene that the inserts would be shorter due to the wear of cutting edges. This strange phenomenon happens because ZOLLER Venturion 600 introduced reference error for each measurement. This reference error has no effects on tool presetting because it does not affect the relative axial positions of the three wiper inserts and the 15 cutting inserts. However, absolute axial positions of wipers edges cannot be obtained due to the reference error. Therefore, a compensation process is needed to acquire the actual axial positions from the measured results.

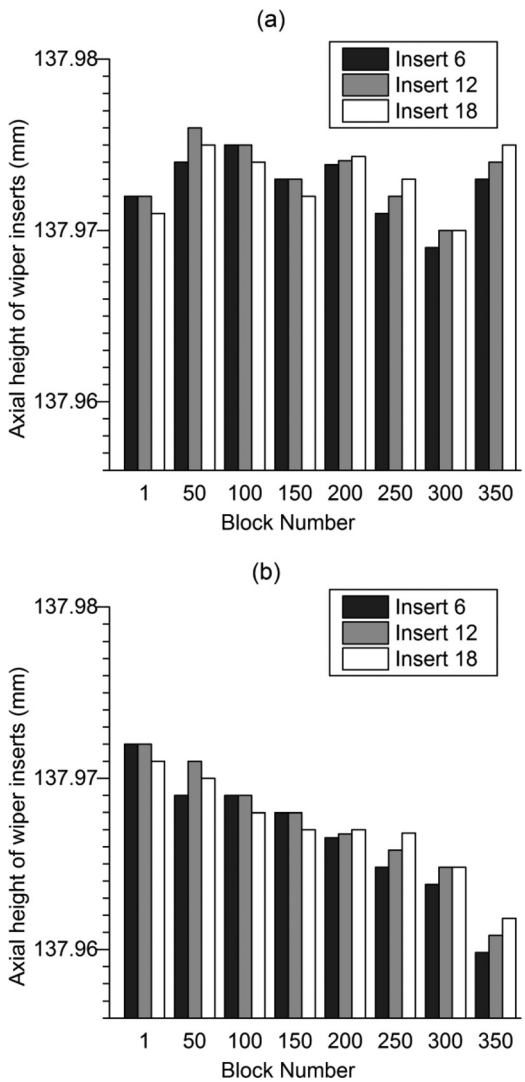

Fig. 4 Axial height of wiper edges versus number of blocks machined: (*a*) measured axial height and (*b*) compensated axial height

Assume that the axial positions of all inserts are lower or equal to the previous positions in the machining process. Therefore, there is a least reference error to make sure that the axial position of each insert is lower or equal to the axial position of the same insert in previous measurement. The least reference error can be used to compensate for the absolute axial positions of the wiper inserts. The least reference error is calculated as follows:

$$E_i = \begin{cases} 0, i = 1 \\ \max\left(z_i^j - z_{i-1}^j\right), \quad i = 2, ..., 8, \quad j = 1, ..., 18 \end{cases} \tag{1}$$

where z_i^j is the ith measured axial position of the jth insert. E_i is the least reference error between the ith measurement and $(i-1)$th measurement. $E_1 = 0$ because the there is no reference error for the first measurement. The range of subscript i is from 1 to 8 because the experiments machined a total of 350 workpiece and measured every 50 workpiece. In addition, the range of superscript j is from 1 to 18 representing the 15 cutting inserts and 3 wiper inserts. The compensated axial positions of the inserts are calculated as follows:

$$Z_i^j = z_i^j - E_i, \quad i = 1, ..., 8, \quad j = 1, ..., 18 \tag{2}$$

where Z_i^j is the compensated axial position of the jth insert for the ith measurement. The compensated axial positions for wiper insert 6, 12, and 18 are shown in Fig. 4(*b*).

The axial lowering of each wiper edge is obtained by calculating the difference between the initial axial positions and the compensated axial positions

$$d_i^j = Z_{i+1}^j - Z_1^j, \quad j = 6, 12, 18 \tag{3}$$

The lowering of the wiper edge in this experiment is calculated as the average lowering of the three wiper inserts, and the results are shown in Fig. 5. The lowering of the wiper edge increased

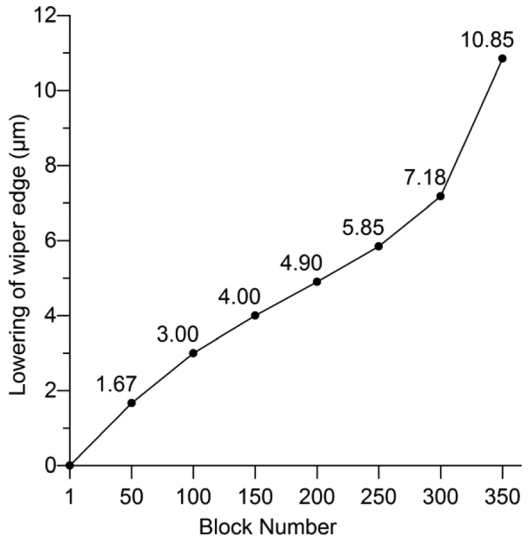

Fig. 5 Average axial lowering of the three wiper inserts

with the number of machined engine blocks. The magnitude of the lowering of the wiper edge was at the scale of micrometer. The lowering value reached 10.85 μm after machining 350 blocks.

3 Extraction of Wear Indicators

This section describes how to extract wiper-wear related indicators from HDM data. The wiper inserts with a wiping flat (also called parallel land) are used to produce featureless surface finish. However, in practical machining situations, wear and axial offsets of wiper inserts make rather complicated surface texture. Wear indicators of wiper inserts can be extracted from 3D surface height map measured by HDM data. The extraction process contains three steps. First, we converted HDM data into a height-encoded gray image that contains all the height and spatial information of the entire surface. Second, the curvilinear toolmarks of the converted image are straightened to ensure equivalent distance between two adjacent toolmarks along the same direction. Finally, we adopted a modified GLCM method to describe the second order statistical information of the machined surface, which avoids boundary distortion. 3D surface form features, including entropy and contrast, are calculated from the modified GLCM along the direction perpendicular to the straightened toolmarks as wear indicators. The correlation of these indicators with wear of wiper inserts was studied in experiments conducted in real industrial environment.

3.1 Gray Image Converting. Raw HMD data contains a large number of data points with noises in both horizontal direction and vertical direction. The HDM data should be preprocessed to a suitable data type for further analysis. Therefore, the HDM data preprocessing method proposed in Ref. [25] was introduced to convert HDM coordinates $[X_i\ Y_i\ Z_i]$ into a height-encoded gray pixel $I(m,n)$ with all the height and spatial information of the raw HDM data. The pixel index (m,n) and pixel gray intensity I are calculated as follows:

$$m = \frac{X_i - X_{\min}}{l}, \quad n = \frac{Y_i - Y_{\min}}{l} \tag{4}$$

$$I(m,n) = \left[\frac{Z_i - S_L}{S_U - S_L} \times 255\right] \tag{5}$$

where l is the resampling interval, S_L and S_U are the lower and upper limits of Z coordinates. Considering lateral resolution of HDM equal to 0.15 mm and flatness specification of engine block surface equal to 0.05 mm, l is set as 0.2 mm and S_L and S_U are set as -0.03 mm and 0.03 mm. Under the same image converting criterion, i.e., the same l, S_L, and S_U, pixel index (m,n) and pixel gray intensity I have the same quantitative relation with the coordinates $[X_i\ Y_i]$ and $[Z_i]$. In other words, gray images measured from different workpiece can be compared and evaluated at the same level. Figure 7(*a*) shows an example of the converted gray image of an engine block surface and its partial enlarged detail.

This quantitative relation between measured points and image pixels is an advantage of HDM-converted images compared with images obtained by machine version in [18,19,28,29]. For HDM-converted image, surface texture can be calculated directly using pixel intensities, whereas for machine-version-acquired image, surface texture is predicted indirectly by correlating pixel intensities with point heights.

3.2 Toolmark Straightening. Surface features related to the wear of wiper inserts are most significant perpendicular to the direction of toolmarks. For face milled surfaces, the directions of toolmarks are changing in one revolution of one insert because the cutting process consists of a translation and a rotation at the same time. Therefore, the distance between two adjacent toolmarks along the same direction is varying at different positions. For example, as shown in Fig. 7(*a*), toolmark distance at the edge and center of the surface is different along the same direction. As a result, surface information of profiles along the same direction at two different positions cannot guarantee the consistent results. To tackle this problem, the curvilinear toolmarks are straightened to straight lines. Thus, wear indicators can be extracted along the perpendicular direction of the straightened toolmarks.

The toolmark straightening procedure described in Ref. [30] is adopted for face milled surfaces with no back cutting. Figure 6 shows one curvilinear toolmark produced by the cutting path of one wiper insert on one revolution. The milling cutter is moving along the cutter path (X axis) at the feed rate f (mm/s) and the rotational speed ω (rad/s). Assume the cutter center is at point O and the wiper insert starts cutting at point A ($t = 0$). After a quarter revolution, the cutting insert intersects with the X axis at point C ($t = t_C$). Then the curvilinear arc AC is the toolmark of one wiper insert.

The curvilinear toolmark can be projected onto a straight line passing through point C and perpendicular to the X axis. For an arbitrary point B on arc AC, the corresponding point on the projected line is written as B'. The coordinates of point B are as follows:

$$\begin{aligned} x_B &= x_O + R\sin\omega t_B + f t_B \\ y_B &= R\cos\omega t_B \end{aligned} \tag{6}$$

Therefore, $t_B = \arccos(y_B/R)/\omega, 0 < t_B < \pi/2\omega$ and $x_O = x_B - f t_B - R\sin\omega t_B$, where R is the cutter radius. The length of $B'C$ should be the same as that of BC. Therefore, the coordinates of point B' are as follows:

$$\begin{aligned} x_{B'} &= x_C = x_O + R + f\frac{\pi}{2\omega} \\ y_{B'} &= \text{length}(BC) = \int_{t_B}^{\pi/2\omega} \sqrt{\left(\frac{dx_B}{dt}\right)^2 + \left(\frac{dy_B}{dt}\right)^2}\, dt \end{aligned} \tag{7}$$

The toolmark straightening process is repeated for all the points on the surface until all the toolmarks are straightened to straight lines. Figure 7(*b*) shows the toolmark-straightened engine block surface. Toolmark distance at the edge and center of the surface is equal along the same direction. Therefore, analyzing surface features from profiles along the same direction at different positions will give consistent results.

3.3 Surface Feature Extracting. A modified GLCM technique is used to analyze the 3D surface form error using the

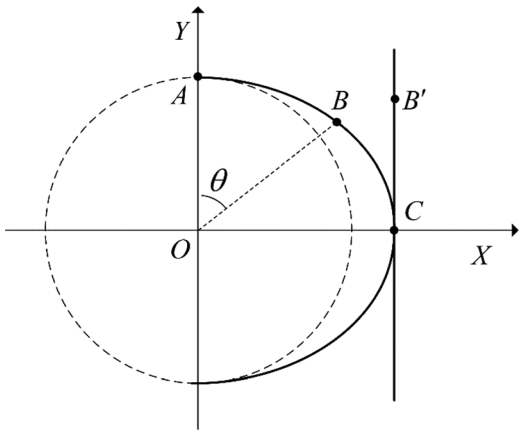

Fig. 6 Face milling toolmark straightening

toolmark-straightened image. GLCM describes the co-occurrence of two pixels for a specified distance and direction [31]. Given the converted gray image $I(x,y)$, the normalized co-occurrence frequencies $p(i,j)$ between gray level i and j are defined as [25]

$$p(i,j) = P(i,j) \Big/ \sum_{i=1}^{N_g} \sum_{j=1}^{N_g} P(i,j) \tag{8}$$

$$P(i,j) = \#\{I(x_1,y_1) = i, \quad I(x_2,y_2) = j, \quad x_2 = x_1 + D\cos\theta, \quad y_2 = y_1 + D\sin\theta\}, \quad i \neq 0, \quad j \neq 0 \tag{9}$$

where N_g is the number of gray levels, i and j are the corresponding gray levels of pixels $I(x_1,y_1)$ and $I(x_2,y_2)$ with the pixel distance D and the pixel angle θ, # denotes the number of pixel pairs satisfying the conditions, and $i \neq 0, j \neq 0$ eliminate the pixel pairs of the nonmeasured area.

The pixel angle and pixel distance should be carefully decided to reflect the subtle changes of the machined surface due to the wear of wiper inserts. As shown in Fig. 6(*b*), surface feature is prominent on horizontal direction of the straightened image. Therefore, pixel angle is taken as 0 deg. The pixel distance is calculated as follows: Considering the cutting speed (1300 rpm), the feed rate (3360 mm/min), and the number of wiper inserts (3), the feed per wiper insert per revolution is $3360/(1300 \times 3) = 0.862$ mm. Given the distance between two adjacent pixels (0.2 mm), the pixel distance between two adjacent toolmark produced by different wiper inserts is at least equal to $0.862/0.2 = 4.31$. Therefore, we choose the pixel distance $D = 5$ to describe the surface feature produced by two adjacent wiper inserts.

From the modified GLCM, two uncorrelated features, entropy and contrast, are derived as wear indicators

$$\text{entropy} = -\sum_i \sum_j p(i,j)\log(p(i,j)) \tag{10}$$

$$\text{contrast} = \sum_{n=0}^{N_g-1} n^2 \left\{ \sum_{i=1}^{N_g} \sum_{\substack{j=1 \\ |i-j|=n}}^{N_g} p(i,j) \right\} \tag{11}$$

Entropy evaluates the randomness of the surface height distribution. Entropy is small for regularly distributed surface height and it is large for randomly distributed surface height. Contrast measures the degree of surface local variation, such as grooves and ridges, which is the amount of local surface height difference between a pixel and its neighbor over the image. The correlation of these indicators with the wear of wiper inserts is discussed in Sec. 4.

4 Results and Discussion

Along with the measurement of the wear of wiper inserts, three successive engine blocks were measured every 50 workpiece by HDM. The modified GLCM is calculated with pixel angle equal to 0 deg and pixel distance equal to 5. Entropy and contrast are the average of the three engine blocks. The averaged entropy and

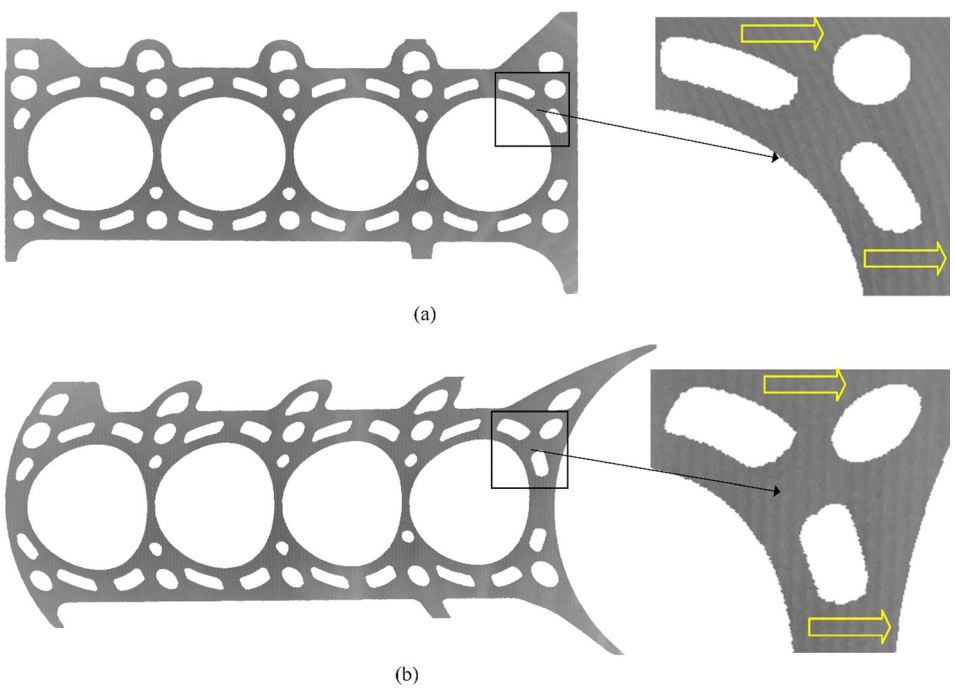

Fig. 7 Height-encoded gray image converted from HDM data: (*a*) original toolmark and (*b*) straightened toolmark

contrast versus number of blocks machined are shown in Figs. 8(*a*) and 8(*b*), respectively.

One of the most consistent observations was that entropy increased with the number of blocks machined and the lowering of the wiper edge. The correlation coefficient between entropy and the lowering of the wiper edge is 0.947, which illustrates that entropy is a good indicator of the lowering of the wiper edge. The high correlation coefficient between entropy and the lowering of the wiper edge is reasonable. On a geometric view, wiper edges became duller along with the lowering of the wiper edge. Thus, the surface randomness and nonuniformity increased and entropy went in the same direction. The strong correlation between entropy and lowering of the wiper edge can be used for the prediction of tool life and control of machining accuracy, allowing the optimum tool change before tool failure.

Knowledge about the lowering rate of wiper inserts versus the machined workpieces can be also used for online tool position compensation. The milling process uses axial position of the wiper edge as tool position reference. Along with the machining progress, the wiper edge becomes lower. The lowing of wiper edge shortens the milling tool and gradually shortens the depth of cut in the axial direction. The shortening of the depth of cut could lead to the surface dimension out of tolerance. If the tool position can be compensated based on the knowledge of lowering rate of the wiper edge, surface dimension would be improved and cutting tools can reach its maximum capability.

A not entirely unexpected finding is that contrast first decreased with machined parts before machining 150 engine blocks and then increased after machining 150 engine blocks. This phenomenon can be explained as follows. As described in Sec. 3, contrast describes the degree of surface local variation. Because the surface local variation is caused by alteration of the depth of cut of the three wiper inserts due to various axial offsets, contrast is likely to be associated with the evolution of axial offset of the three wiper inserts in the milling process. The axial offset of wiper inserts is determined by the initial axial position and individual wear rate for each wiper insert. As can be seen in Fig. 4(*b*), at the beginning of machining, wiper inserts 6 and 12 were higher than insert 18. As wiper insert 6 and 12 wore more quickly than wiper insert 18, the three wiper inserts tended to have the equal axial positions, i.e., small axial offset. Therefore, the local variation caused by axial offset of the three wiper inserts became smaller and contrast became lower. After machining 150 parts, the wear rate of wiper insert 6 and 12 was still higher than that of wiper insert 18. Therefore, axial offset of the three wiper inserts became larger again, so contrast increased.

In addition to monitoring the cutting tool wear, the experimental results can also help increase the cutting tool life. As shown in Fig. 4(*b*), the wear rates of all the three wiper inserts were different, which could cause the early changing of cutting tool due to

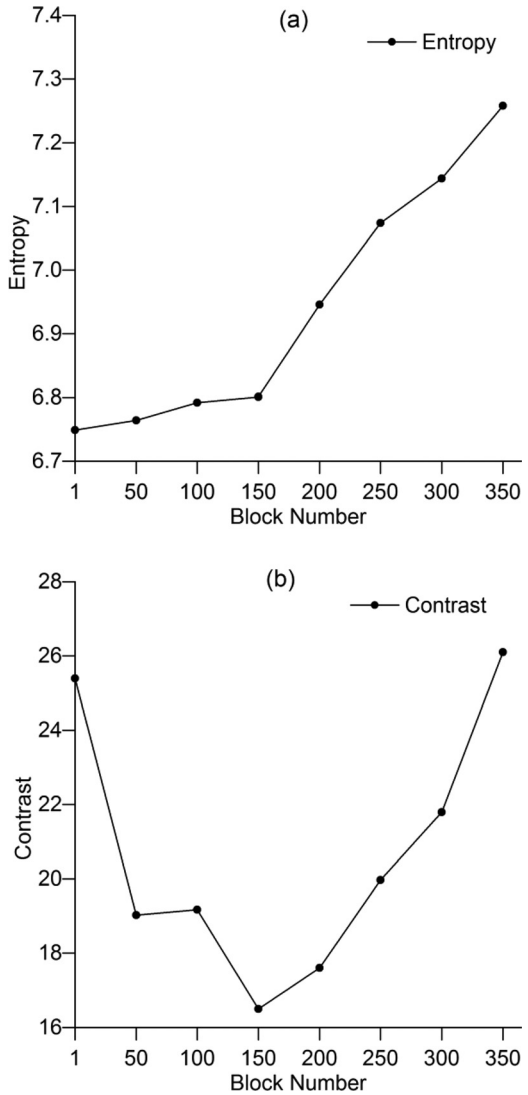

Fig. 8 (*a*) entropy versus number of blocks machined and (*b*) contrast versus number of blocks machined

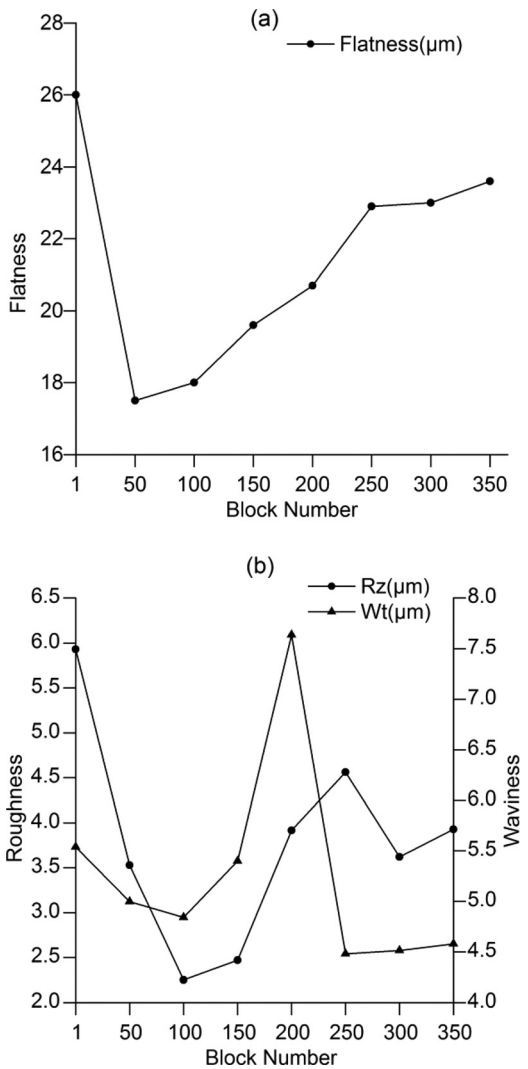

Fig. 9 (*a*) Flatness versus number of blocks machined and (*b*) roughness and waviness versus number of blocks machined

the failure of one particular wiper insert. Therefore, tool life can be increased by balancing the different wear rate of wiper inserts. In general, the wear rate of wiper inserts would result from the different cutting load or cutting allowance. Therefore, balancing the cutting allowance of wiper inserts by presetting the relative axial and radial positions between the wiper insert and its five precedence cutting inserts can help increase the tool life.

Flatness, roughness, and waviness were also measured to test their ability for monitoring the wear of wiper inserts in multi-insert face milling. Flatness was averaged from the HDM data of the three sampled engine blocks for each measurement. As can be seen in Fig. 9(*a*), flatness showed a tendency to increase with the number of blocks machined except at the initial cutting period. Therefore, flatness did not always provide consistent values that can be related to the wear of wiper inserts. Roughness (Rz) and waviness (Wt) were measured at eight different positions for the three sampled engine blocks using a Hommel T8000 instrument. The results shown in Fig. 9(*b*) were an average of the measured values. As can be seen, roughness (Rz) and waviness (Wt) were not always reliable tool wear indicators. This is because roughness and waviness are affected by multiple factors including radial and axial offsets between inserts, wear, runout, mechanical impact, transient thermal stresses, and back cutting. Even for the same workpiece, the measurement of roughness and waviness can vary substantially for different measuring positions and directions.

Besides face milling process, other surface machining processes such as end milling and grinding can be monitored using the proposed method. For certain machined surfaces with no clear toolmarks, surface features could be extracted from the HDM converted image using the modified GLCM technique without toolmark straightening. At the same time, it would be possible to define a direction locally for extracting GLCM features, given that the tangent to the surface height gradient is readily found. Extensive experiments are required to establish the correlation between the extracted surface features and the tool wear condition.

5 Conclusions

This work presented a wear monitoring method for wiper inserts in multi-insert face milling using 3D surface form as tool wear indicators. The 3D surface form indicators including entropy and contrast were extracted from height-encoded and toolmark-straightened gray images that contain the entire 3D surface topography information. The wear of wiper inserts was represented using the axial lowering of the wiper edge, which was measured using a tool presetter and measuring machine without dismounting wiper inserts from the cutter. Experimental results indicated that entropy showed a strong correlation with the axial lowering of the wiper edge and contrast was related to the evolution of axial offset between multiple wiper inserts. These findings can be used to control multi-insert milling accuracy by compensating tool positions and increase tool life through proper inserts setting. In future work, we plan to focus on the repeatability study of various feed rate, cutting speed, and insert mounting patterns and on monitoring marked wear of wiper inserts.

Acknowledgment

This work was supported by the National Science & Technology Pillar Program of China (2012BAF06B03), the National Natural Science Foundation of China (51275558), the Programme of Introducing Talents of Discipline to Universities (B06012), the Fund for Innovative Research Groups of the National Natural Science Foundation of China (51121063), Shanghai Rising-Star Program (Grant No. 13QA1402100), and China Postdoctoral Science Foundation funded project (2014M561465). All experiments were performed at SAIC GM Wuling Automobile (SGMW); we are grateful to SGMW engineers for their experimental support.

Nomenclature

D = pixel distance
d_i^j = axial lowering of the wiper edge
E_i = least reference error between two measurements
f = feed rate
$I(m,n)$ = height-encoded gray pixel
l = resampling interval
N_g = number of gray levels
$p(i,j)$ = normalized co-occurrence frequencies
R = cutter radius
S_L, S_U = lower and upper limit of Z coordinates
Z_i^j = compensated axial position of one insert
z_i^j = axial position of one insert
θ = pixel angle
ω = rotational speed

References

[1] Roth, J. T., Djurdjanovic, D., Yang, X., Mears, L., and Kurfess, T., 2010, "Quality and Inspection of Machining Operations: Tool Condition Monitoring," ASME J. Manuf. Sci. Eng., **132**(4), p. 041015.
[2] Pfeifer, T., and Wiegers, L., 2000, "Reliable Tool Wear Monitoring by Optimized Image and Illumination Control in Machine Vision," Measurement, **28**(3), pp. 209–218.
[3] Jurkovic, J., Korosec, M., and Kopac, J., 2005, "New Approach in Tool Wear Measuring Technique Using CCD Vision System," Int. J. Mach. Tools Manuf., **45**(9), pp. 1023–1030.
[4] Kerr, D., Pengilley, J., and Garwood, R., 2006, "Assessment and Visualisation of Machine Tool Wear Using Computer Vision," Int. J. Adv. Manuf. Technol., **28**(7–8), pp. 781–791.
[5] Castejón, M., Alegre, E., Barreiro, J., and Hernández, L. K., 2007, "On-Line Tool Wear Monitoring Using Geometric Descriptors From Digital Images," Int. J. Mach. Tools Manuf., **47**(12–13), pp. 1847–1853.
[6] Shahabi, H. H., and Ratnam, M. M., 2009, "In-Cycle Monitoring of Tool Nose Wear and Surface Roughness of Turned Parts Using Machine Vision," Int. J. Adv. Manuf. Technol., **40**(11–12), pp. 1148–1157.
[7] Wang, X., and Kwon, P. Y., 2014, "Wc/Co Tool Wear in Dry Turning of Commercially Pure Aluminium," ASME J. Manuf. Sci. Eng., **136**(3), p. 031006.
[8] Oraby, S. E., Al-Modhuf, A. F., and Hayhurst, D. R., 2004, "A Diagnostic Approach for Turning Tool Based on the Dynamic Force Signals," ASME J. Manuf. Sci. Eng., **127**(3), pp. 463–475.
[9] Kious, M., Ouahabi, A., Boudraa, M., Serra, R., and Cheknane, A., 2010, "Detection Process Approach of Tool Wear in High Speed Milling," Measurement, **43**(10), pp. 1439–1446.
[10] Kaya, B., Oysu, C., and Ertunc, H. M., 2011, "Force-Torque Based On-Line Tool Wear Estimation System for CNC Milling of Inconel 718 Using Neural Networks," Adv. Eng. Software, **42**(3), pp. 76–84.
[11] Alonso, F. J., and Salgado, D. R., 2008, "Analysis of the Structure of Vibration Signals for Tool Wear Detection," Mech. Syst. Signal Process., **22**(3), pp. 735–748.
[12] Kilundu, B., Dehombreux, P., and Chiementin, X., 2011, "Tool Wear Monitoring by Machine Learning Techniques and Singular Spectrum Analysis," Mech. Syst. Signal Process., **25**(1), pp. 400–415.
[13] Jesús, R.-T. R. D., Gilberto, H.-R., Iván, T.-V., and Carlos, J.-C. J., 2003, "Driver Current Analysis for Sensorless Tool Breakage Monitoring of CNC Milling Machines," Int. J. Mach. Tools Manuf., **43**(15), pp. 1529–1534.
[14] Salgado, D. R., and Alonso, F. J., 2007, "An Approach Based on Current and Sound Signals for in-Process Tool Wear Monitoring," Int. J. Mach. Tools Manuf., **47**(14), pp. 2140–2152.
[15] Marinescu, I., and Axinte, D. A., 2008, "A Critical Analysis of Effectiveness of Acoustic Emission Signals to Detect Tool and Workpiece Malfunctions in Milling Operations," Int. J. Mach. Tools Manuf., **48**(10), pp. 1148–1160.
[16] Yen, C.-L., Lu, M.-C., and Chen, J.-L., 2013, "Applying the Self-Organization Feature Map (SOM) Algorithm to Ae-Based Tool Wear Monitoring in Micro-Cutting," Mech. Syst. Signal Process., **34**(1–2), pp. 353–366.
[17] Attanasio, A., Ceretti, E., Giardini, C., and Cappellini, C., 2013, "Tool Wear in Cutting Operations: Experimental Analysis and Analytical Models," ASME J. Manuf. Sci. Eng., **135**(5), p. 051012.
[18] Dutta, S., Datta, A., Chakladar, N. D., Pal, S. K., Mukhopadhyay, S., and Sen, R., 2012, "Detection of Tool Condition From the Turned Surface Images Using an Accurate Grey Level Co-Occurrence Technique," Precis. Eng., **36**(3), pp. 458–466.
[19] Kassim, A. A., Mannan, M. A., and Mian, Z., 2007, "Texture Analysis Methods for Tool Condition Monitoring," Image Vis. Comput., **25**(7), pp. 1080–1090.
[20] Wilkinson, P., Reuben, R. L., Jones, J. D. C., Barton, J. S., Hand, D. P., Carolan, T. A., and Kidd, S. R., 1997, "Surface Finish Parameters as Diagnostics of Tool Wear in Face Milling," Wear, **205**(1–2), pp. 47–54.
[21] Dutta, S., Pal, S. K., Mukhopadhyay, S., and Sen, R., 2013, "Application of Digital Image Processing in Tool Condition Monitoring: A Review," CIRP J. Manuf. Sci. Technol., **6**(3), pp. 212–232.

[22] ISO, ISO 25178-602:2010, 2010, *Geometrical Product Specifications (GPS)—Surface Texture: Areal—Part 602: Nominal Characteristics of Non-Contact (Confocal Chromatic Probe) Instruments*, ISO, Geneva, Switzerland.
[23] Huang, Z., Shih, A. J., and Ni, J., 2006, "Laser Interferometry Hologram Registration for Three-Dimensional Precision Measurements," ASME J. Manuf. Sci. Eng., **128**(4), pp. 1006–1013.
[24] Liao, Y., Stephenson, D. A., and Ni, J., 2010, "A Multifeature Approach to Tool Wear Estimation Using 3D Workpiece Surface Texture Parameters," ASME J. Manuf. Sci. Eng., **132**(6), p. 061008.
[25] Wang, M., Xi, L., and Du, S., 2014, "3D Surface Form Error Evaluation Using High Definition Metrology," Precis. Eng., **38**(1), pp. 230–236.
[26] de Souza, A. M., Jr., Sales, W. F., Santos, S. C., and Machado, A. R., 2005, "Performance of Single Si_3N_4 and Mixed Si_3N_4+PCBN Wiper Cutting Tools Applied to High Speed Face Milling of Cast Iron," Int. J. Mach. Tools Manuf., **45**(3), pp. 335–344.
[27] Astakhov, V. P., 2004, "The Assessment of Cutting Tool Wear," Int. J. Mach. Tools Manuf., **44**(6), pp. 637–647.
[28] Al-Kindi, G., and Zughaer, H., 2012, "An Approach to Improved CNC Machining Using Vision-Based System," Mater. Manuf. Process., **27**(7), pp. 765–774.
[29] Dutta, S., Kanwat, A., Pal, S. K., and Sen, R., 2013, "Correlation Study of Tool Flank Wear With Machined Surface Texture in End Milling," Measurement, **46**(10), pp. 4249–4260.
[30] Nguyen, H. T., Wang, H., and Hu, S. J., 2013, "Characterization of Cutting Force Induced Surface Shape Variation in Face Milling Using High-Definition Metrology," ASME J. Manuf. Sci. Eng., **135**(4), p. 041014.
[31] Haralick, R. M., Shanmugam, K., and Dinstein, I. H., 1973, "Textural Features for Image Classification," IEEE Trans. Syst. Man Cybern., **3**(6), pp. 610–621.